UC San Diego

UC San Diego Electronic Theses and Dissertations

Title

Spatial and temporal structure of the fog life cycle over Atlantic Canada and the Grand Banks

Permalink

Author

Formby-Fernandez, Adriana

Publication Date

2023

Peer reviewed|Thesis/dissertation

UNIVERSITY OF CALIFORNIA SAN DIEGO

Spatial and temporal structure of the fog life cycle over Atlantic Canada and the Grand Banks

A thesis submitted in partial satisfaction of the
requirements for the degree Master of Science

in

Oceanography

by

Adriana Denise Formby-Fernandez

Committee in charge:

    Luc Lenain, Chair
    Clive Dorman
    Jennifer Mackinnon
    Nicholas Pizzo
    Shang-Ping Xie

2023

The thesis of Adriana Denise Formby-Fernandez is approved, and it is acceptable

in quality and form for publication on microfilm and electronically.

University of California San Diego

2023

DEDICATION

This thesis is dedicated to my support system who helped me throughout this journey: friends, family, and myself. The creation of this masterpiece taught me a lot about myself and for that I am proud.

EPIGRAPH

Low-anchored cloud,
Newfoundland air,
Fountain head and source of rivers,
Dew-cloth, dream drapery,
And napkin spread by fays;
Drifting meadow of the air,
Where bloom the daisied banks and violets,
And in whose fenny labyrinth
The bittern booms and heron wades;
Spirit of the lake and seas and rivers,
Bear only perfumes and the scent
Of healing herbs to just men's fields!

Henry David Thoreau

TABLE OF CONTENTS

LIST OF FIGURES

LIST OF TABLES

ACKNOWLEDGEMENTS

I would like to acknowledge Luc Lenain for his support as the chair of my committee and as an excellent advisor and mentor. Through multiple drafts and many long coding days, his guidance has proved to be invaluable.

I would also like to acknowledge Nicholas Pizzo for his support as a co-advisor and co-mentor. His guidance has helped me become a better scientist and a better life-long student.

My final acknowledgment goes to my cohort and lab mates for their endless help with my research, their endless support through my journey, and for brightening up my time here. They were the best part of this master's degree.

VITA

2021   Bachelor of Arts, Embry-Riddle Aeronautical University, Daytona Beach

2023   Master of Science in Oceanography, University of California San Diego

ABSTRACT OF THE THESIS

Spatial and temporal structure of the fog life cycle over Atlantic Canada and the Grand Banks

by

Adriana Denise Formby-Fernandez

Master of Science in Oceanography

University of California San Diego, 2023

Luc Lenain, Chair

Marine fog impacts human health, naval strategy, and biological productivity. Despite its importance, the skill of operational and global environmental models in forecasting marine fog and its optical properties remain limited due to our incomplete understanding of the physical processes that drive fog, particularly over its broad range of temporal and spatial scales. The Gulf Stream and the Labrador Sea currents meet in Atlantic Canada and the Grand Banks off

Newfoundland, Canada, making it a productive region for biodiversity with a wide range of physical oceanographic features present. This region has one of the two highest fog occurrences in the world (Dorman et al., 2020). In this work, we present findings from a 71-year climatological analysis covering a broad range of spatial and temporal scales. Using ICOADS observations from 1950-2020, ERA5 reanalysis products, and satellite imagery, we discuss fog formation and annihilation in this region. Spatially, the Atlantic Canada continental shelf induces submesoscale ocean features along its rapid variation in bathymetry. These structures influence the fog life cycle. Sharp sea surface temperature gradients and air-sea temperature differences coincide with the over-the-shelf fog maxima in summer (June, July and August). The air-sea temperature differences show a clear signal that fog occurrence is higher with negative air-sea temperature differences (SST - air temperature). This higher occurrence of fog is mainly isolated on the continental shelf, where colder SST typically exists. Temporally, climatological trends confirm correlations between air-sea temperature differences and high fog occurrence within sample regions on and off-shelf. Satellite imagery of a fog event during the 2022 ONR FATIMA MURI campaign highlights the complicated interplay of shelf break dynamics and near-surface atmospheric conditions. A fog bank is shown to form in the colder water regions over the shelf, outlining the shelf break and pointing to boundary layer and smaller-scale processes that are driving fog formation. These observations are crucial in characterizing the spatial and temporal structure of the fog life cycle and provide a better understanding of fog occurrence in this region.

Chapter 1

1.1 Introduction

Despite its societal importance, our understanding and ability to predict fog, whether in coastal, offshore or in land environments remains limited. This is in part due to complexity of the physical processes driving the fog life cycle and the observational challenges of characterizing processes that span a broad range of spatio-temporal scales (i.e. synoptic to microphysical turbulence scales). As fog reduces visibility at sea, improved understanding of the small-scale structure of fog, including aerosol, droplet and turbulence properties, is necessary in order to better forecast the propagation of optical and radio-frequency electromagnetic signals critical to operations at sea (both for aircraft and vessels).

Fog is defined as a collection of airborne water particles or ice crystals of magnitude $5\text{-}50\mu m$ that collectively reduce visibility to less than 1 km near the Earth's surface (Gultepe et al., 2007). Fog can exist over land or water and has been categorized into 11 main types (Willett, 1928; Byers, 1959) depending on formation mechanism and location. This study explores advection marine sea fog, which occurs when warmer, higher humidity air is advected over colder sea surface regions (Gultepe et al., 2007). The warmer air cools and condenses to become fog, extending from the ocean surface to several hundreds meters in height (see Figure 1.1). The fog

life cycle is constrained by a range of multiscale processes both in the atmosphere and at the air-sea boundary: radiative cooling at the fog top, the evolution of surface heat and turbulent moisture fluxes resulting from flows over ocean fronts, and other variations in turbulence within the cloud (Findlater et al., 1989; Yang and Gao, 2020). Radiative cooling and turbulent mixing of the overlaying warm air leads to a more thermally stable internal boundary layer. This persists because the turbulent thermal interface, which exists a few hundred meters above the surface, divides the marine layer into two regions: 1) a turbulent layer near the sea surface, and 2) a thermal radiation turbulent layer from long-wave cooling from the fog top (Koračin et al., 2014). Vertical mixing increases within the marine boundary layer (MBL) when air blows over a warm-to-cold SST front. This allows the MBL to deepen and allows for more entrainment at the top of the MBL (Skyllingstad et al., 2007).

Fog formation is influenced by a combination of synoptic large scale weather patterns (Koračin and Dorman, 2017) and small-scale, local microphysical processes, making fog prediction and modeling particularly challenging (see, e.g. Wainwright and Richter, 2021; Chen et al., 2021; Pithani et al., 2019; Taylor et al., 2021; Hu et al., 2014; Park et al., 2022). Typically atmospheric temperature decreases with height. A temperature *inversion* exists when temperatures above the sea surface increase with height. During normal summer conditions over the ocean, a low-level, near surface temperature inversion exists with unsaturated air parcels. This marine boundary layer is stable, such that convective motions between the layers are not expected (Nieuwstadt, 2005). Within the boundary layer, horizontal movement of warm air over colder water creates and maintains an air temperature inversion, creating a stratified layer between the sea surface and the boundary layer above. As winds blow across a SST gradient, as shown in Figure 1.1, the entire boundary layer cools, not just that with the surface air temperature inversion. The result is as the boundary layer is advected with the flow of the wind, the entire boundary layer cools as the sea surface cools so that saturation is not achieved. If the dominant mean condition is a moist but unsaturated surface-based air temperature inversion, with dryer air
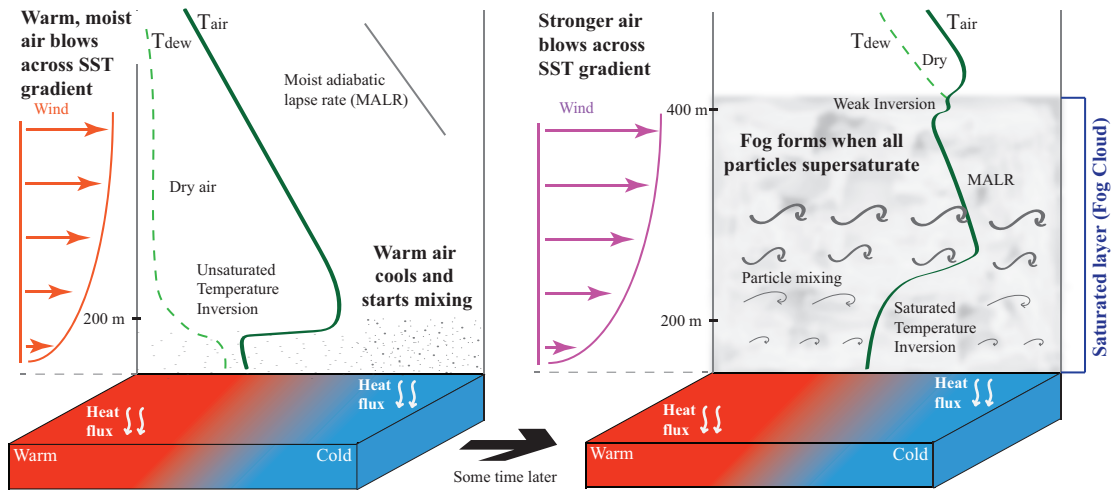
Figure 1.1. Simplified schematic of warm advection sea fog formation over a cold boundary, like a shelfbreak. In the first panel, normal summer conditions are shown: low-level unsaturated temperature inversion with dry air aloft, and cooling particles that are not saturated. The second panel shows conditions favorable for fog following an atmospheric trigger: a saturated, low-level temperature inversion below a weaker inversion with dry air aloft. Stronger and more turbulent wind causes particle mixing within a deeper and saturated layer in which fog can form.

above, winds from the warm side of the SST gradient with wind shear and turbulence increasing from the sea surface upward, then a trigger is needed to convert this mean unsaturated surface air temperature inversion, to a saturated surface air temperature inversion. This trigger could be a mid-level trough axis crossing overhead, causing surface convergence in the boundary layer and an increase in the surface wind speed and greater wind shear in the boundary layer. The result is that the moist surface air temperature inversion is converted to a deeper, saturated surface air temperature inversion and a saturated layer with a saturated adiabatic lapse rate in the upper portion of the saturated layer. This saturated layer is much deeper than the preceding, unsaturated but moist air temperature inversion. Finally, there can be a weak saturated air temperature inversion

at the top of the saturated layer. Above this, there may be a dry, unsaturated air temperature inversion. Extending from the dry air temperature inversion capping the saturated dry air, or directly extending upward from the top of the saturated layer itself, the air temperature follows a moist adiabatic lapse rate and the air is unsaturated. The transition from unsaturated to a saturated surface boundary layer is not well documented, however the horizontal convergence and shear turbulence are believed to be a factor. In any event this usually occurs within a stable surface layer wherein moisture is moved upward in a stable layer to cause saturation, which defies conventional expectations. This process through narrow layers that are temporarily unstable, with K-H billowing and mixing that moves moisture upward, can make the layer return to being stable, in a process described in Fernando et al. (2023). When the surface and atmospheric conditions are met, fog is formed.

To the north of the Gulf Stream and the Kuroshio currents are the world's most fog-prone regions (Dorman et al., 2017). These regions coincide with sharp ocean sea-surface temperature (SST) gradients and regions of energetic submesoscale activity. The Grand Banks of Newfoundland, Canada, on average experiences fog over 40% of June, July, and August with the greatest occurrences over the continental shelf (Dorman et al., 2020). This is a dynamically rich region of the western Atlantic, with cold water from the Labrador Current meeting the warmer waters of the Gulf Stream. These currents then interact with the continental shelf and predominant southwesterly atmospheric winds which advect relatively warm air over these cooler waters. In discussing a trip to the Grand Banks region in 1917, G.I. Taylor (Taylor, 1917) noted that he experienced 141 events of fog within the 804 days of the trip (including transit time to and from England). Prior to this, other accounts going back as far as 1823 (Scoresby, 1823) and 1907 (Brodrick, 1907) comment on the consistency of fog in the Grand Banks region during the summer. However, detailed spatial and temporal remote and in-situ measurements of these conditions were not historically available, motivating large field programs recently to study the fog life cycle through the lens of both synoptic meteorologists and micro-scale atmospheric

scientists (Dorman et al., 2020, 2021; Wainwright and Richter, 2021; Isaac et al., 2020; Gultepe et al., 2009; Dimitrova et al., 2021; Fernando et al., 2021) with the aim of understanding fog dynamics.

Several recent projects, such as the Fog and Turbulence Interactions in the Marine Atmosphere (FATIMA) project, the C-FOG project (Fernando et al., 2021), and the Fog Remote Sensing and Modeling (FRAM) project (Gultepe et al., 2009) have set out to improve understanding of fog dynamics and forecasting through a better understanding of the impact of smaller scale processes on the fog life cycle. FRAM was a three-part field campaign that explored continental and coastal fog in Canada in which in-situ and remote sensing observations were collected. C-FOG was a multidisciplinary project that sought out to investigate coastal fog from multiple lenses, including air-sea interaction processes, thermodynamics, microphysics, and dynamics. This campaign included a field deployment in Nova Scotia and Newfoundland, from September to October 2018, in which various instruments collected atmospheric and oceanic variables to include in improved numerical models of the fog life cycle. C-FOG was able to highlight the need for further implementation of fog physics at smaller scales into models and forecasting schemes. This project led to the ONR funded FATIMA MURI program, that included a field campaign in that same region in July 2022 to explore fog from synoptic to microphysical scales. In-situ observations were collected during the foggiest time of year in this region, for optimal conditions to investigate the fog life cycle.

Figure 1.2 shows the fog occurrence for July in the Grand Banks computed from 71 years (1950-2020) of ICOADS archived observations. We find that fog occurs up to 60% of the time in some areas, primarily on the continental shelf. The link between the location of high fog occurrence and the boundary of the shelf break motivates this work. In particular, understanding the oceans' role in providing a crucial surface boundary condition to the atmosphere is vital to being able to understand this phenomenon as completely as possible (Fallmann et al., 2019).

5
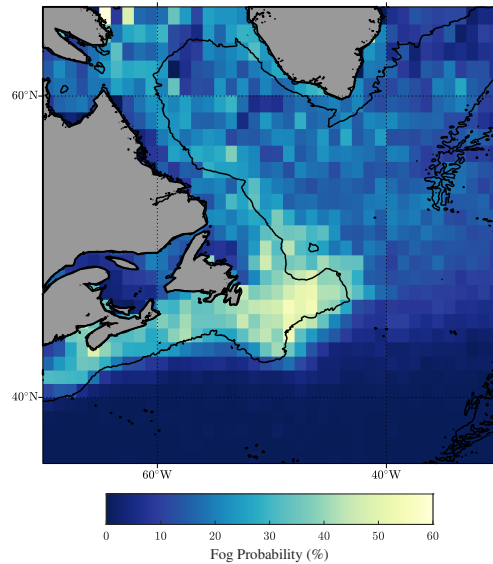
Figure 1.2. July fog occurrence from ICOADS data spanning from 1950-2020. Data was averaged into 1°boxes. The 2000 m bathymetry is outlined in black.

1.1.1 Oceanographic context of the Grand Banks region

The Atlantic Canada shelf is positioned at a crucial interface in the earth climate system where very different water masses, from the colder fresher Labrador Current water, the warmer Labrador Sea water and the warm Gulf Stream water interacts above and along the continental shelf break, leading to highly complex and variable dynamical interplay that modulates the regional ecosystem (Loder, 1998; Richardson et al., 2001; Talley, 2011; Ricketts et al., 1931; Fratantoni and Pickart, 2007; Clarke et al., 1980; Sheng and Thompson, 1996; Han et al., 2011). The Labrador Current brings in cold and fresh water from the Labrador Sea into the Grand Banks region (Fratantoni and Pickart, 2007; Clarke et al., 1980) over the Scotian Shelf, and south towards Cape Hatteras (Figure 1.3). There are two main outflow points, the first one at Flemish Pass (northern edge of the Grand Banks) and the second one at the Tail of the Grand Banks (at the southern edge) (Fratantoni and Pickart, 2007; Petrie and Anderson, 1983).
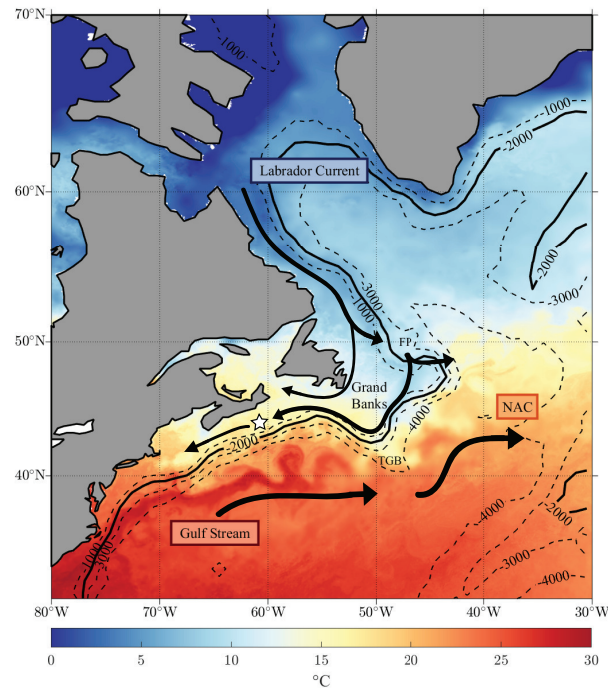
Figure 1.3. Mean SST map from GHRSST MUR showing the Labrador Current and Gulf Stream interaction over the Grand Banks from July 10, 2022 2100Z to July 11, 2022 2100Z. Additional current flow is shown with black lines and arrows. Contour lines for bathymetry are set for every 1000m down to 4000m. The 2000m depth contour is slightly thicker, as this will be the reference contour for the rest of the paper. NAC: North Atlantic Current; FP: Flemish Pass; TGB: Tail of the Grand Banks. The white star is over Sable Island.

The current that dominates the southern part of this region is the Gulf Stream, which becomes the North Atlantic Current (NAC) further to the east (Clarke et al., 1980). The Gulf Stream splits into three branches: 1) a southward stream that goes equatorward along the outer boundary of the original Gulf Stream, 2) a southeastward portion of the North Atlantic Current that eventually becomes the Azores Current, and 3) a northeastward portion that becomes the North Atlantic Current. This third branch is the most relevant to this study, as this is the section closest to the Grand Banks (Talley, 2011). As the Gulf Stream swings north and east, it splits into smaller features, such as the Mann Eddy, the North Recirculation Gyre, and other eastward propagating currents. This splitting of the Gulf Stream induces complex dynamics involving smaller scale

processes. The meanders and jets associated with the Gulf Stream Extension are highly energetic. Figure 1.3 shows some of these meanders and jets occurring just south of the Grand Banks. As the surface currents are driven northward due to winds, this warmer, saltier water is able to mix and interact with the colder shelf water. This creates a region where mesoscale and energetic submesoscale activity is heightened and supported. With the presence of sharp, submesoscale features (McWilliams, 2016) found near the continental shelf (Bower et al., 2013), increased air-sea interactions is expected (Su et al., 2018). These air-sea interactions involve the exchange of heat between the two boundaries. In particular, it has been established that the air-sea temperature difference is a driving mechanism for advection fog formation (Gultepe et al., 2007; Wainwright and Richter, 2021; Isaac et al., 2020; Dorman et al., 2020).

This study aims to provide a larger picture view of the multi-scale air-sea interactions that are associated with the fog life cycle, that are driven by these air-sea temperature differences. This paper presents a novel outlook on advection sea fog through a 71-year climatological analysis of fog occurrence and its necessary components over the Grand Banks region coupled with a small-scale investigation of an individual fog event over Sable Island. It is important to evaluate the impact that the surface conditions have on fog so models and forecast schemes can accurately predict this phenomenon. We find that the ocean plays a crucial role in the fog life cycle through its impact on the surface boundary conditions needed for advection sea fog formation.

Section 2 explains the data and methods used in this study. Following this will be the results in Section 3. Section 4 summarizes and discusses the findings from this paper.

1.2   Data and Methods

A combination of in-situ (e.g. ship, autonomous vehicles, platforms, buoys) and remote sensing observations are used in this analysis, along with two reanalysis products (ERA5 and ORA5). They are described below.

1.2.1 ICOADS

Following the approach of Dorman et al. (2020), we used archived observations as part of the International Comprehensive Ocean and Atmospheric Dataset (ICOADS) (Freeman et al., 2017) v3.0.0. This archive combines global in-situ observations collected from ships, buoys, and other ocean-based platforms since 1662. Here we use a subset of observations spanning from January 1, 1950 through December 31, 2020 over the region of Grand Banks and the northwest Atlantic, from 35-65°N and 30-70°W. Sampling rates varied greatly throughout the span of the record, ranging from subhourly to 3-hour intervals. Due to the nature of the dataset, being a combined record from all vessels in the area, some observations occurred within a few seconds of each other, while others were taken only daily. For this analysis, the time sampling was not an issue as data is averaged monthly. See the appendix and Figure A.2 for more information. Monthly average maps of selected variables are over a 1°x 1°grid, while observations from on and off the shelf are averaged spatially in different subregions to analyze the temporal evolution of the state variables and fog over the course of the 71-year record. To compute fog occurrence, we divide the number of present weather observations categorized as "fog" (ICOAD codes 40-49) over the total amount of present weather observations within the 1°x 1°grid box. These codes follow from the WMO Code Table 4677 (WMO, 2019; Dorman et al., 2020). The 2000 m depth contour is used to identify the location of the continental shelf break in the figures.

The ICOADS observations are quality controlled using the NCDC QC flags. Specific thresholds to remove outliers are added as a secondary check. These criteria are shown in Table 1.2. Observations where sea surface temperature (SST) and surface air temperature (SAT) is above 35°C or below -5°C are removed. The difference between SST and SAT (ΔT) is also limited to -10°and 10°C. The surface wind speed upper threshold is set at 30m/s to limit contributions from energetic storms in the climatology.

An example of an ICOADS produced map for July from 1950-2020 is shown in Figure

1.4 for fog occurrence, SST, SAT, and winds. Figure 1.4a shows the highest amount of fog occurrence concentrated on the Grand Banks continental shelf. The SST (Figure 1.4b) and SAT (Figure 1.4c) plots show the signatures of colder water and surface air temperatures that occur on the shelf and to the north of the Grand Banks. The warm Gulf Stream is clearly seen to the south of the shelf in the deeper water in this region. Unadjusted wind speed is shown in Figure1.4d with the directionality of the wind overlaid in white. Though wind speed observations are known to exhibit an upward trend due to the increasing height of ship-based measurements (Tokinaga and Xie, 2011; Cardone et al., 1990; Thomas et al., 2008), this does not impact the spatial climatology presented here. We find wind speeds on the shelf to be slightly lower than off the shelf, particularly in the region to the eastern side of the Grand Banks.
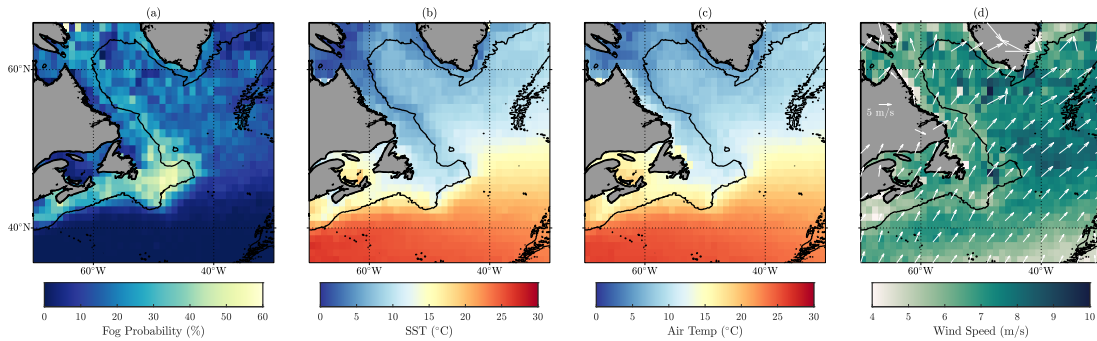
Figure 1.4. ICOADS July maps from averaged 1°x 1°boxes across 71 years of data. (a) Fog Occurrence. (b) Average SST per grid point in °C. (c) Average Air Temperature per grid point in °C. (d) Unadjusted wind speed (m/s) per grid point is shown in the background with wind vectors on top. Wind speeds taken from ICOADS are subject to height measurement bias. The 2000m depth contour is shown.

1.2.2 ECMWF ERA5 and ORA5 reanalysis products

The ICOADS dataset is augmented with hourly, gridded products from the ECMWF Reanalysis v5 (ERA5) (Hersbach et al., 2020) products for 1950-2020. A list of all considered variables is included in Table 1.1. Additional ocean state products are also obtained from the ORAS5 Global ocean reanalysis monthly data from 1958-2020 (Zuo et al., 2018). All reanalysis data is averaged through all years for each corresponding month within a 0.25°by 0.25°grid box.

Table 1.1. ICOADS variables used with their respective resolutions. The time resolution is variable due to the nature of the dataset being collected from many vessels. See the appendix and Figure A.2 for more information. ERA5 single level data is taken from the surface (or lowest level available). ERA5 pressure level data includes all the levels in the atmospheric model. ORAS5 data is taken from 0-10 m depth.

Period Covered	Time Resolution	Grid Resolution	Variable	Units
		ICOADS v3.0.0		
1950-2020 (except Salinity, 1950-2014)	Variable (see the appendix)	1°x 1°	SST	°C
			Air Temperature	°C
			Present Weather (WW)	N/A
			Wind Speed (W)	m s^{-1}
			Wind Direction (D)	°
			Salinity (OSV)	g/kg
		ERA5 Single Level		
1950-2020	Hourly	0.25°x 0.25°	SST	°C
			Air Temperature	°C
			Surface Latent Heat Flux	kW m^{-2}
			Surface Sensible Heat Flux	kW m^{-2}
		ERA5 Pressure Levels		
1950-2020	Hourly	0.25°x 0.25°	Air Temperature	°C
			Air Pressure	mb
		ORAS5		
1958-2020	Monthly	0.25°x 0.25°	Potential Temperature	°C
			Salinity	PSU

Table 1.2. Quality check and additional thresholds and criteria set on the ICOADS data to ensure storm bias and other errors were not included in the analysis.

ICOADS v3.0.0		
Variable	Quality Check Variable	Threshold Criteria
SST	SNC	-5 to 35 °C
Air Temperature	ANC	-5 to 35 °C
Present Weather (WW)	XNC	Fog Code = 40-49
Wind Speed (W)	WNC	0-30 m s^{-1}
Wind Direction (D)	WNC	N/A
Salinity (OSV)	N/A	0-10 m depth

1.2.3 ONR FATIMA 2022 field program

The first campaign of the ONR FATIMA MURI program occurred from July 3rd to August 3rd, 2022 in the Grand Banks, combining observations from a research vessel, autonomous surface vehicles (Grare et al., 2021), and an extensive suite of atmospheric sensors installed on Sable Island, including a ceilometer CL31 used in the present analysis.

1.2.4 GOES geostationary satellite (GOES-16) observations

Geostationary Operational Environmental Satellites (GOES) 16 is a satellite operated by NASA and the National Oceanic and Atmospheric Administration (NOAA). GOES-16 serves as the operational geostationary weather satellite in the GOES East position at 75.2°W, providing a view centered on North America, extending to the Atlantic and Pacific oceans with a nominal 2km and 5min spatial and temporal resolution. GOES-16 provides observations both in the visible and infrared wavelength through 16 spectral bands (Advanced Baseline Imager - ABI). Following the approach of Amani et al. (2020), we use two of these ABI bands, the thermal infrared ($\sim$11μm) and mid-infrared ($\sim$3.9μm), to compute brightness temperature difference

by subtracting the thermal infrared band by the mid-infrared band. The thermal infrared band shows a higher brightness temperature for fog than the mid-infrared band, but clouds appear the same in both. After subtracting the two bands, clouds are removed and fog can be more clearly seen, if there are no clouds above the fog layer. The algorithm is modified to enable daytime fog detection by adjustments made to the detection threshold.

1.3   Results

Fog climatology over the Grand Banks region

Observational data from 1950-2020 from ICOADS is analyzed spatially to characterize the climatology of fog within this region. Figure 1.5 shows the fog occurrence (Figure 1.5a) for the month of July along with a map of air-sea temperature difference (Figure 1.5b). The air-sea temperature difference (ΔT) is defined as the difference between SST and surface air temperature. We find that fog occurs up to 60% in some areas on the shelf, with the extent of the region where fog is most prevalent generally following the edge of the continental shelf, in particular to the south of the banks. Very limited occurrence of fog is found south of the shelf. At that time of the year, wind (purple arrows) is generally coming from the southwest, with monthly averaged wind speed ranging from 1 to 14 m/s, bringing warm air above the much colder waters present on the shelf. The air-sea temperature map follows a similar trend, with negative values (down to $-2°C$) on the shelf, and positive off the shelf (up to $+2°C$) showing a remarkable correlation between the locations of the continental shelf break and the region where the air-sea temperature difference changes sign.

We focus here on the climatology for the months of May, June, July, and August as fog are most prevalent in this region at that time of the year. Figure 1.6 shows the fog occurrence and air-sea temperature differences, with each column corresponding to a different month: May, June, July, and August. Fog occurrence is highest in July (Figure 1.6c, up to 60%), concentrated on the shelf, as previously discussed. Note that, as compared to the other months, a significant amount
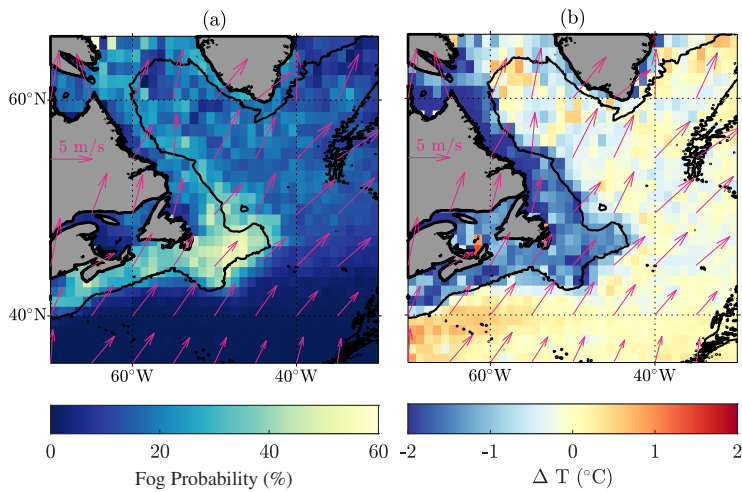
Figure 1.5. July (a) fog occurrence, (b) air-sea temperature differences (ΔT) show the spatial correlation with each other and the bathymetry. Wind direction is overlaid in pink. The 2000 m depth contour is shown.

of fog (20-25%) also occurred in the higher latitudes within the Labrador Current, hinting at either the role of local submesocale processes in this region extending away from the shelf or due to synoptic scale patterns interacting with the land and the ocean. Fog occurrence remains limited off the shelf to the south of Grand Banks. In Figure 1.6, we find that negative air-sea temperature differences coincide with areas of high fog occurrence in each of the months. Fog occurrence drops significantly from July to August, also coinciding with a decrease in the magnitude of the air-sea temperature difference, associated with a slow seasonal warming of the waters on the shelf.

In Figure 1.7, fog occurrence for the month of July is sorted as a function of air-sea temperature difference (ΔT) ranges. Due to the small amount of observations available in the grid points in the northern part of the region, grid boxes with less than 10 observations have been removed. We find that the maximum percentage of fog occurrence occurs within the ΔT range of -3 to -4°C. As the magnitude of the temperature difference increases, the probability of fog occurrence decreases. Overall, fog occurs more frequently when the temperature gradient across the air-sea interface is largest. This is partly due to the transfer of heat, in which cooler water

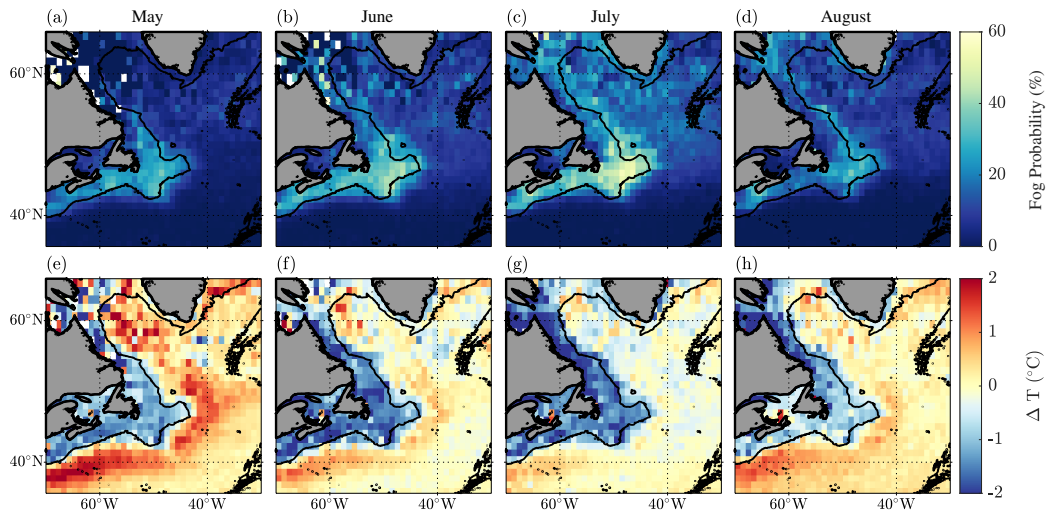**Figure 1.6.** Spatial and temporal variability of fog occurrence (top row) and air-sea temperature difference (ΔT, second row). The air-sea temperature difference is defined as the SST minus the surface air temperature. The first column is for May, second is for June, third is for July, and the fourth column is for August. The 2000 m depth contour is shown.

chills the air particles above it, making them condense, release more latent heat, and increase their buoyancy. As these particles become more buoyant, they rise eventually forming a stably stratified layer in which fog can form. The threshold for this temperature gradient has been experimented with through LES models (Wainwright and Richter, 2021). In July, warmer air from the Gulf Stream tends to blow over the Grand Banks, and thus intensifies the negative air-sea temperature differences which can cause greater fog occurrence. Nevertheless, we also find occurrences of fog when air colder than the ocean blows over the region (f-h). This could be caused by different fog mechanisms and dynamics, which we did not explore in this study. Note, regardless of the air-sea temperature difference range, fog is limited to occurrence on the continental shelf in the southern part of the region, where the SST tends to have a sharper gradient.

Surface salinity, wind speed, and direction are shown in Figure 1.8 for May through August. We find that winds are consistently coming from the southwest throughout the summer season. These winds originate from over the Gulf Stream and/or over the continental US, where they are

15
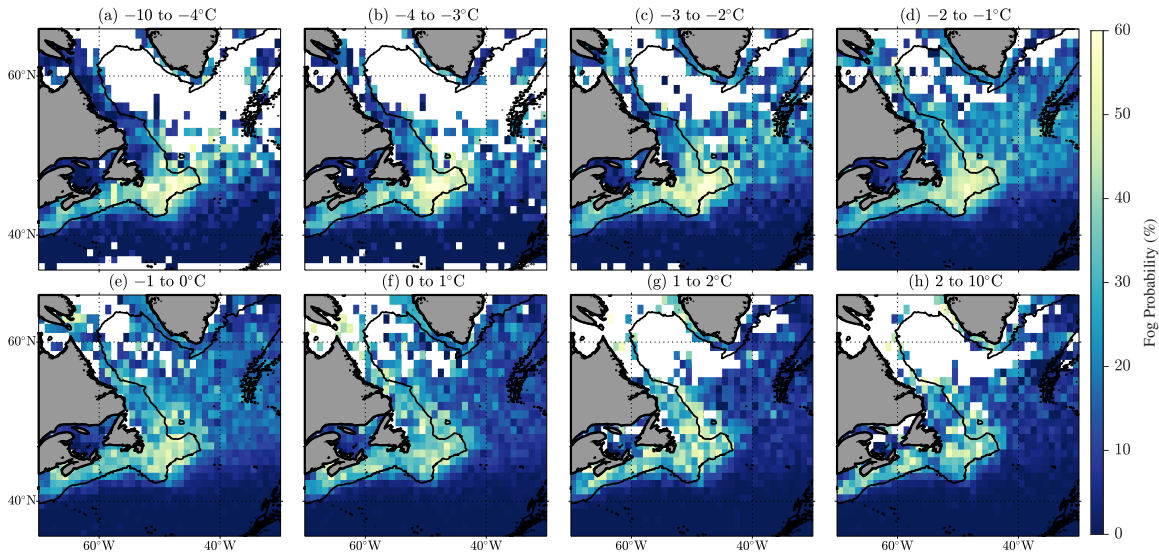
Figure 1.7. Fog occurrence with respect to varying air-sea temperature difference (ΔT) values for July. Grid boxes with less than 10 points removed. ΔT ranges vary as follows: (a) -10°C to -4°C, (b) -4°C to -3°C, (c) -3°C to -2°C, (d) -2°C to -1°C, (e) -1°C to 0°C, (f) 0°C to 1°C, (g) 1°C to 2°C, (h) 2°C to 10°C. The 2000 m depth contour is shown.

blowing warmer air over the GB region. Wind speed in the region gradually decreases from May through July then increases again slightly in August. Note the clear reduction of surface wind speed within or at the shelf break for each one of these months. Surface salinity remains generally uniform during these four months (Figure 1.8e-h). The water on shelf is fresher, consistent with a difference in density associated with the interaction between the Labrador Current water to the north and the Gulf Stream water to the south. The on shelf water tends to get slightly fresher as the season goes on. This is likely due to contribution from summer melting of sea ice to the north, freshwater discharge from the rivers, and general seasonal advection of the fresher Labrador Current water further south (Hu and Zhao, 2022).

As the water on the shelf continues to warm throughout the season, the difference in temperature from the air brought in by the southwesterly winds and the ocean sea surface

Figure 1.8. Spatial and temporal variability of wind speed and direction (top row) and salinity (second row). Each column correspond to a monthly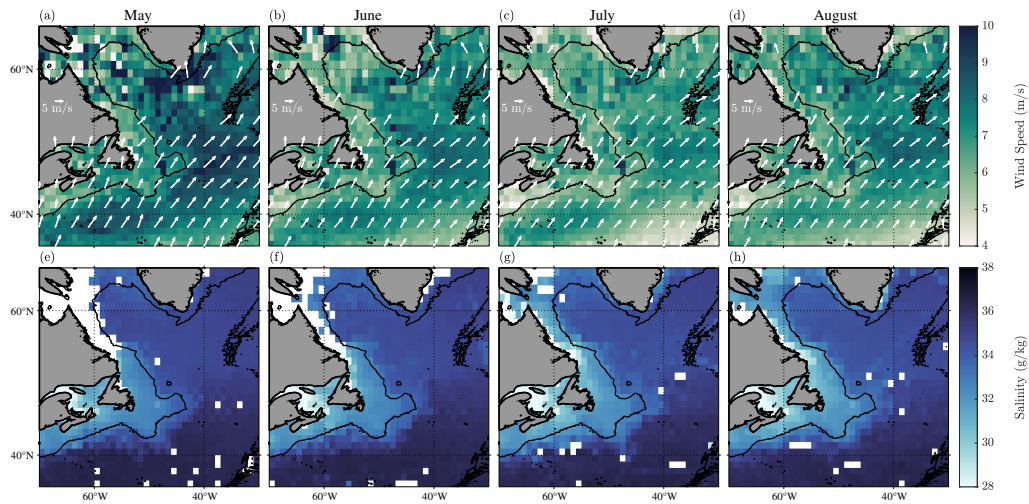 average, from May through August. The 2000m depth contour is shown. Wind direction arrows in grid boxes with less than 400 observations have been removed.

temperature decreases. The monthly-averaged winds vary only slightly in magnitude and direction between July and August, hinting at the role of ocean surface conditions in driving fog generation during the summer season. When this air-sea temperature difference becomes smaller in magnitude (less negative, or zero), the marine boundary layer becomes more neutral, decreasing convective motion within the layer, and limiting fog formation. As the air-sea temperature difference becomes positive, the marine boundary layer is considered unstable and advection sea fog formation continues to be limited.

1.3.1 Atmospheric boundary layer and surface fluxes

Monthly averaged surface latent and sensible heat fluxes obtained from ERA5 over the 71-year record are shown in Figure 1.9. Note, these fluxes are positive into the ocean. The positive latent heat flux corresponds to conditions where water is condensing in the lowest section of the atmosphere, and negative values show evaporation from the sea surface. On the shelf, we find surface latent heat flux to be generally positive, consistent with an active area of fog formation, as fog particles are releasing latent heat through condensation (Severini et al.,

17
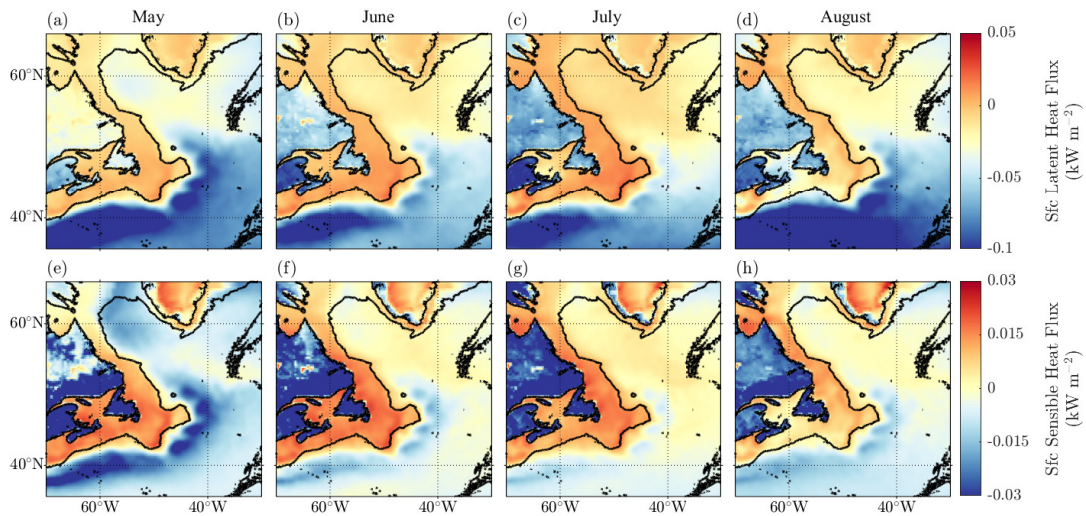
Figure 1.9. Surface Latent Heat Flux (kw m^{-2}) (top row) and Surface Sensible Heat Flux (kw m^{-2}) (bottom row) for May to August from 1950-2020 from ERA5. Positive fluxes are into the ocean. The 2000 m depth contour is shown.

1986). Conversely, the negative values outlining the Gulf Stream to the south show an area with evaporation.

The role of sensible heat flux in the context of the fog life cycle has been extensively studied (e.g. (Yang et al., 2019; Thompson et al., 2005; Yun and Ha, 2022). Positive sensible heat flux within fog or cloudy conditions acts as dissipation of the feature. Again, positive values are into the ocean for this analysis. We see in the bottom row of Figure 1.9 that higher positive values of surface sensible heat are found on the shelf, correlated with the areas of negative air-sea temperature differences and high fog occurrence. In particular, the surface sensible heat flux denotes areas where fog dissipation is occurring more frequently. Since fog formation and dissipation happen on time scales on the order of a fraction of an hour to a few days, it is not surprising to find both positive sensible and latent heat fluxes on the fog prone region on the shelf. South of the shelf, we find negative sensible heat fluxes, which show were the Gulf Stream brings warm water to that region.

Fog formation depends critically on the presence of an inversion layer in the lower at-
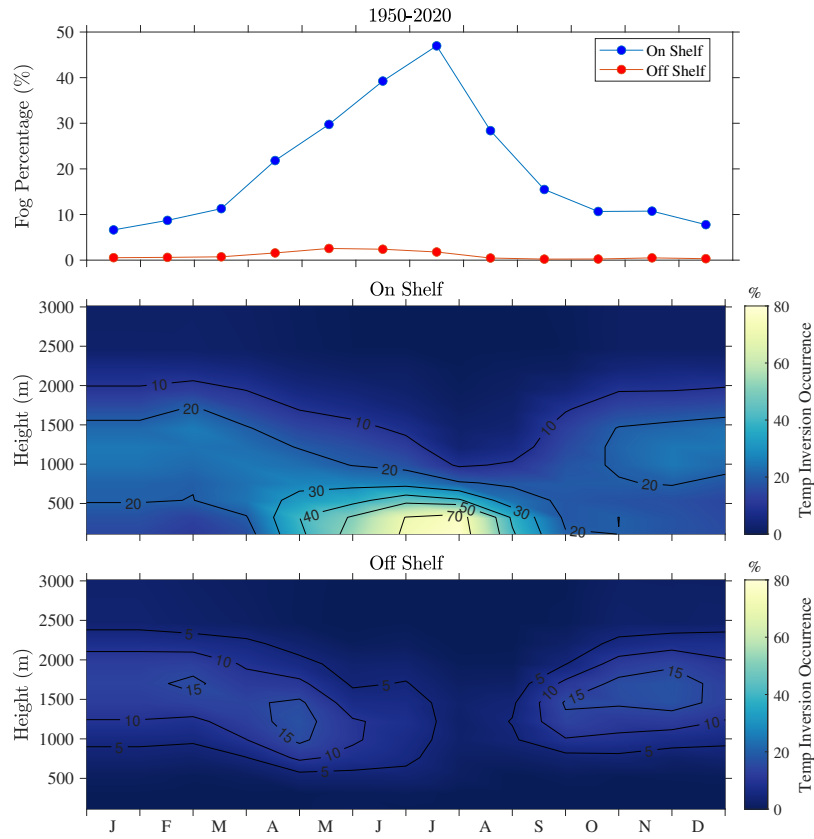
Figure 1.10. Occurrence of temperature inversions per month for 71 years over two new subregions. The on-shelf region spans 45°N to 48°N and -48°W to -51°W. The off-shelf region spans 39°N to 42°N and -52°W to -55°W. (a) The fog probability of occurrence for these two subregions from ICOADS data. (b) The on-shelf probability of occurrence of temperature inversions from ERA5 data. (c) The off-shelf probability of occurrence of temperature inversions from ERA5 data.

mospheric boundary layer (Koračin et al., 2014; Dorman et al., 2017, 2020). In Figure 1.10, ERA5 atmospheric profiles show the probability of hourly occurrence of temperature inversions averaged per month over the 71-year record considered. For each hourly atmospheric profile, the pressure levels during which a temperature inversion ($\frac{dT}{dz} > 0$) occurred is identified. The fraction of times when this occurrs is then computed per month. Two smaller subregions on and off the shelf are used in the analysis. The on-shelf fog-prone subregion spans from 45°N to 48°N and -48°W to -51°W. The off-shelf subregion is chosen upwind of the shelf at 39°N to

42°N and -52°W to -55°W. On the shelf (Figure 1.10b), we find significant seasonality in the occurrence of temperature inversions, up to 80% likelihood to occur at levels below 500m during the summer months. On the contrary, off the shelf (Figure 1.10c), upstream of the Grand Banks, we find limited occurrence of temperature inversions, up to 15%, and at much larger altitudes (1000-2000m) throughout the year. The inversions are quasi nonexistent off the shelf during the summer months.

Over the fog prone region of the Grand Banks, evidence supports the existence of moisture advection from evaporation and winds, heat fluxes that support fog formation and dissipation, and temperature inversions during the summer season. The consistent spatial pattern across these variables, along with those shown in Figure 1.5, point to the predominance of summer fog in that region.

1.3.2 Temporal climatology

To characterize the temporal evolution of fog occurrence and bulk state variables on and off the shelf, ICOADS observations are averaged over two regions chosen based on the JJA fog occurrence and SST products described above. The boundaries of the on-shelf fog-prone region are selected as the area on the continental shelf where the fog percentage is over 20%. The off-shelf "warm" region boundaries are selected to be over the warmest SST region, within the Gulf Stream. The off-shelf boundaries are from 43°W to 63°W and 35°N to 39°N. Figure 1.11 shows the on and off-shelf regions overlaid on the respective plot where the criteria is set (JJA fog occurrence and SST map, respectively).

Figure 1.12 shows ICOADS observations averaged over the summer months (June, July, August) for on (black) and off (blue) shelf for the fog occurrence, air-sea temperature difference (ΔT), SST, and air temperature from 1950 to 2020. We find significant year-to-year variability of fog occurrence averaged over the shelf over the summer months, from 20 to 50%. The fog appeared to be occurring more often after 1984 (30-50% range), while some of the lowest
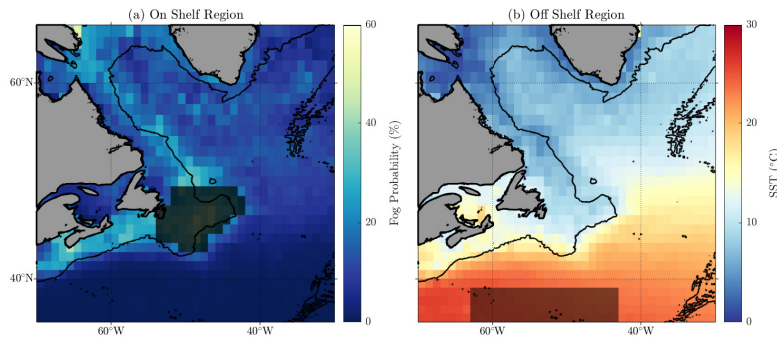
Figure 1.11. Two subregions are created to provide a comparison of "cold, foggy" conditions and "warm, clear" conditions. (a) The on-shelf region as determined by grid points where fog percentage is over 20% in JJA. (b) The off-shelf region as determined by the warmest SST regime in JJA. The 2000 m depth contour is shown.

values are found prior. Recent studies have shown that some regions have seen an uptick in fog occurrence due to increased pollutants and anthropogenic aerosols in the atmosphere (Yan et al., 2019), and changing synoptic-scale patterns (Fonseca et al., 2023). Other regions have seen decreases of fog over the last few decades (Johnstone and Dawson, 2010; Vautard et al., 2009; Akimoto and Kusaka, 2015).

Off the shelf, JJA averaged air-sea temperature differences (ΔT, Figure 1.12b) slowly decrease from 1960 to 1990, from approximately $+0.5°C$ to $-0.5°C$, then trending upward through the 2010s. On the shelf, the air-sea temperature differences (ΔT) are mostly negative with significant year-to-year variability. The negative magnitude is concurrent with the spatial analysis shown above.

Sea surface temperature (Figure 1.12c) and surface air temperature (Figure 1.12d) exhibit similar trends in both regions considered. Off the shelf, they both show an upward trend, approximately $+2°C$ for the SST and $+4°C$ for the surface air temperature from 1970 to 2020. On the shelf, we find much larger year-to-year variability making long-term trends harder to identify. This is likely caused by the meandering of the Gulf Stream and the interaction with

the Labrador Current shelf water from the north in the small region where these averages are computed. The change in trends for the SST and air temperature in the 1970s-1980s off the shelf has been investigated by Chen et al. (2020). They attributed this upward trend in temperature to both multidecadal variability and an externally forced warming trend.

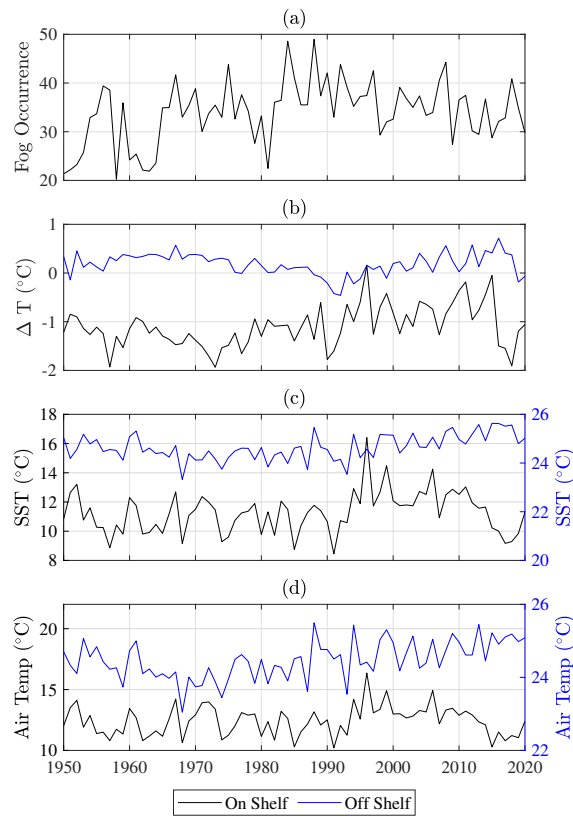**Figure 1.12.** June, July, and August data averaged per year for (a) fog occurrence, (b) air-sea temperature difference (ΔT, °C), (c) SST (°C), and (d) surface air temperature (°C). On shelf data is in black, and off shelf data is in blue.

Smaller scales seem to be dominating the interannual and intraseasonal variability. A smaller spatial scale analysis is investigated in the next part of this paper.

1.3.3 High-resolution observations of a fog event near Sable island during the FATIMA field experiment

To investigate the smaller-scale impacts of the surface conditions on fog, high resolution observations of an individual fog event are analyzed. Figure 1.13 shows the averaged SST taken from July 10-12, 2022 from GOES-16 satellite imagery during the FATIMA 2022 experiment. The mean SST is computed by averaging brightness temperature (ABI band 14) for areas not contaminated by clouds or fog over the 48h considered. Though the 2-day averaging leads to some smearing, we can identify submesoscale features such as filaments and fronts. The warmer waters typically follow the shelf break though submesoscale features extend to the north and south of it. Submesoscale features are also located throughout the region shown. This includes the colder water on the shelf, and around Sable Island, where island wakes are present.
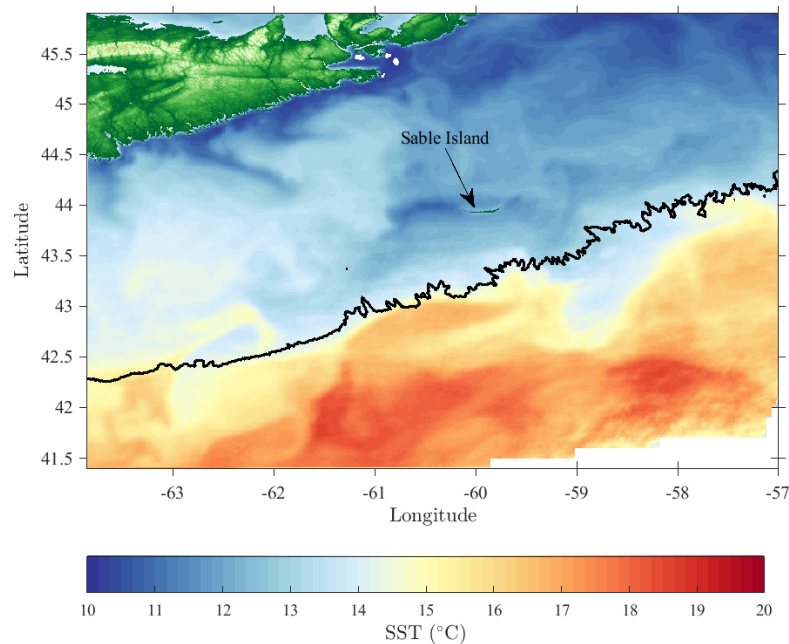

Figure 1.13. Mean SST around Sable Island from GOES-11 satellite imagery over July 10-12, 2022 with the 2000 m depth contour in black.

A ceilometer mounted at the South Tower in Sable Island provided observations of the

structure of the atmospheric boundary layer during the experiment. Measurements collected from July 10, 2022 00:00 UTC to July 11, 2022 06:00 UTC are shown in Figure 1.14(a), identifying an initially intermittent shallow fog layer (20-150m in height) that lasted for close to 30 hours.

Fog spatial extent, computed from the GOES imagery product, along with coincident and collocated in-situ imagery of fog conditions collected from the South Tower at Sable Island are presented for specific times (07/10/2022 17:47 UTC, 07/10/2022 20:06 UTC, 07/10/2022 23:32 UTC, 07/11/2022 01:01 UTC, and 07/11/2022 03:32 UTC) in Figure 1.14(i-iv). The red dot in the satellite imagery to the left represents the location of Sable Island, while the white dot represents the position of an instrumented wave glider deployed as part of the experiment (Grare et al., 2021); White arrows are used to show wind direction and relative magnitude during these times. The fog extent is overlaid on top of the mean SST presented in Figure 1.13. Both orbital, in-situ and visual imagery products were collected at the same time.

(i) 07/10/2022 17:47 UTC: The ceilometer captured a fog event where the cloud extends from the surface up to about 130m. The orbital product shows a fog bank extending from the shelf break up to the north of Sable Island with weak northerly winds. Fog is visually observed on the camera, though it is spatially inhomogeneous.

(ii) 07/10/2022 20:06 UTC: The fog bank has dissipated over the island, as shown in the ceilometer and visual observations. Nevertheless, camera imagery shows the presence of a fog bank off the island, consistent with the orbital product still showing presence of fog around the island. It appears that fog has dissipated over the island, as the land surface conditions experienced significant daytime warming, annihilating (locally) this fog bank. Note the extent of the fog bank to the south starting to move south of the shelf break southeast of Sable Island.

(iii) 07/10/2022 23:32 UTC: A well-defined fog bank has reformed, approximately 90m high,

much more uniform as compared to the observations earlier in the day. The extent of the fog bank (left column) now follows the structure of the underlying SST, with the fog bank extending to the south of the shelf break.

(iv) 07/11/2022 01:01 UTC: During the earlier part of the evening, the height of the fog bank decreased to about 15m at Sable Island. The lateral extent of the fog bank continues to follow the structure of the SST, stopping at the warmer water to the south. Fog aerosols are visible in the camera imagery though interpretation is limited at night.

(v) 07/11/2022 03:02 UTC: The fog bank started dissipating from the north, with no fog observed at Sable Island from the camera and ceilometer.

In these observations of an individual fog event, we find that the fog extent follows the location of strong gradients of SST more so than the location of the shelf break, in contrast to the statistics discussed in the previous sections. This is summarized in Figure 1.15, where the location of the continental shelf break, and the contour of more than 17% fog occurrence is plotted over the 48 hours of observations considered here. These results hint at the rapid response to the change in the surface boundary conditions, i.e. submesoscale features such as front and filaments, present near the shelf break. The changes in the surface boundary conditions are likely affecting the marine boundary layer processes at play.

1.4   Conclusion/Discussion

In this study, we present a spatio-temporal climatology of fog probability of occurrence and its sufficient components in the Atlantic Canada region from 1950-2020. Using archived in-situ observations, reanalysis products, and remote sensing observations, we explore the influence of multi-scale air-sea interaction processes on the fog life cycle in the Grand Banks.

We show that fog occurs most during the summer months in the Atlantic Canada and Grand

Figure 1.14. Fog characterization from GOES imagery over Sable Island from July 10-11, 2022. (a) Ceilometer data taken from the South Tower at Sable Island, (i)-(iv) (left) Satellite imagery of fog clouds where Sable Island is the red dot, the white dot is a waveglider, wind directions are shown by the arrows, and background mean SST from Figure 1.13 is also plotted. Five specific times during the event are shown, correlating with the dashed lines in (a). (right) Visual imagery from a camera on the South Tower at Sable Island at similar times as the satellite imagery.

(a) (i) (ii) (iii) (iv) (v)
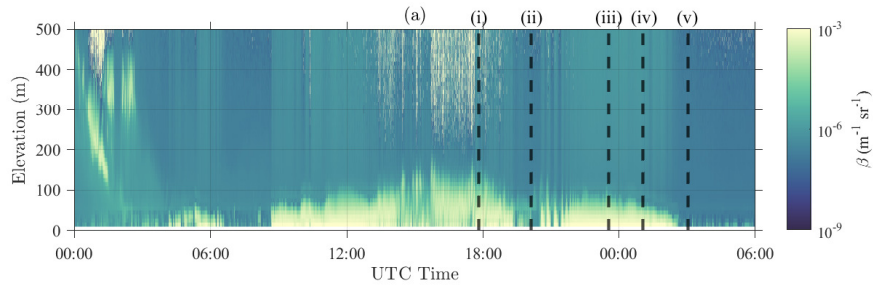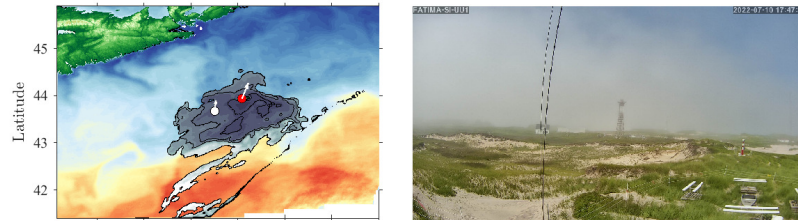
(i) 07/10/2022 17:47

(ii) 07/10/2022 20:06
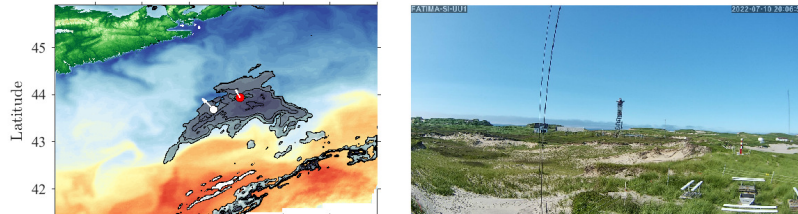
(iii) 07/10/2022 23:32

(iv) 07/11/2022 01:02

(v) 07/11/2022 03:02

27
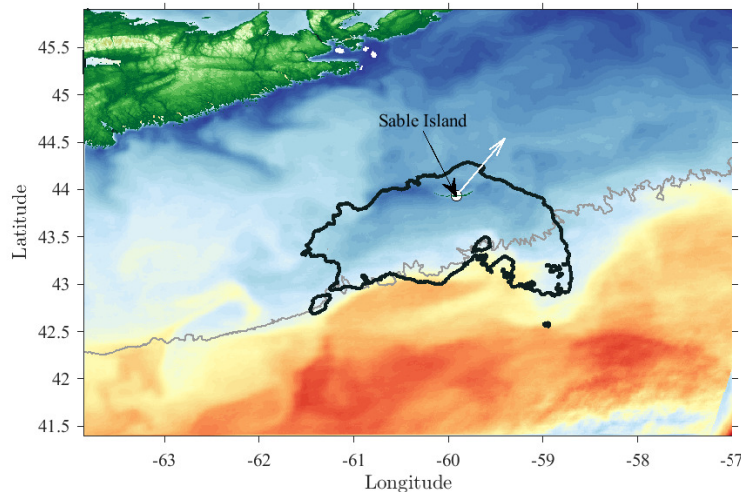
Figure 1.15. Fog contour showing the fog occurrence over the course of 48 hours. The black contour shows areas where fog was present for 17% or more of the time. The white arrow denotes average wind direction during these 48 hours. Note that the fog bank stays in the colder water on the shelf. The 2000 m depth contour is shown in grey.
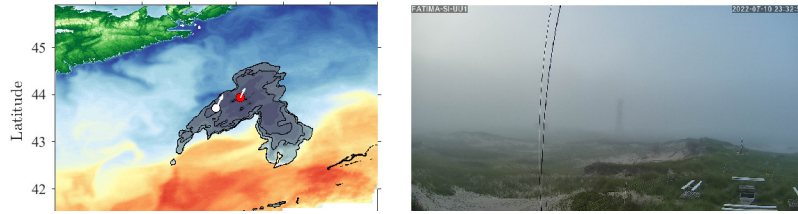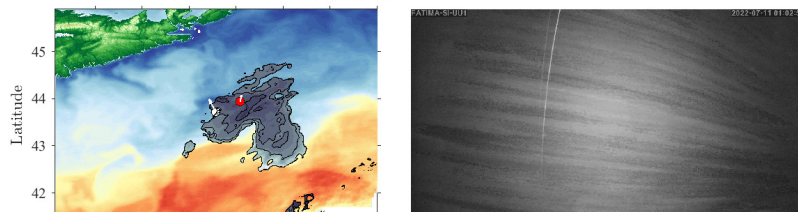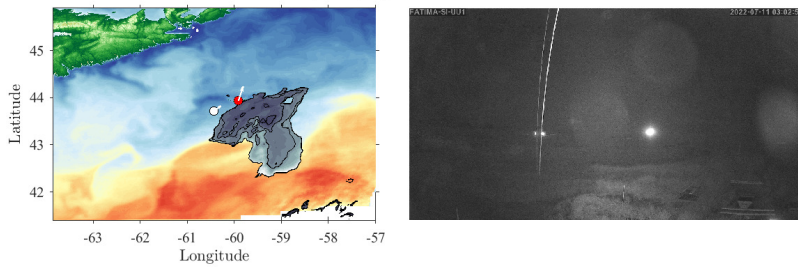
Banks region, highly concentrated along the continental shelf and correlated with the bathymetry. The fog probability of occurrence increases from May to July, reaching up to 60% in localized areas. In August, the probability decreases to below 40%, remaining concentrated on the shelf. Similarly, a strong negative air-sea temperature difference is also correlated with the bathymetry in this region. We find that the fog probability of occurrence increases as the magnitude of the air-sea temperature difference strengthens, as shown in Figure 1.6 from May to July. As the fog occurrence decreases in August, the air-sea temperature difference becomes closer to 0. The highest occurrence coincides with an air-sea temperature difference between -3 to -4°C. Fog still occurs up to 50% of the time with a neutral and/or positive air-sea temperature difference, indicating that fog in this region is also driven by different mechanisms not explored in this study. Fog does not form in the southern part of this region, where the SST tends to be the

warmest, around the Gulf Stream. The presence of an air-sea temperature difference is related to the stability of the marine boundary layer, as it aids or inhibits fog formation. Therefore, an air-sea temperature difference is a necessary condition to be considered in fog parameterizations.

From an atmospheric perspective, two other essential conditions for fog formation include surface winds bringing warmer air over the colder ocean region and the existence of low-level atmospheric temperature inversions above this region. During the summer, winds on average are directed from the southwest, bringing warmer air from over the Gulf Stream above the colder shelf water and Labrador Current waters to the north. From May to July, wind speeds tend to decrease. From July to August, the wind speed increases and the wind direction varies slightly, which points to a different mechanism causing the fog occurrence to decrease. Above the surface, there is a high occurrence of low-level atmospheric temperature inversions (over 70%) during the summer, which are also found to occur primarily on the shelf. These inversions occur over 50% of the time from May to August below a height of 500 m. Upwind of the shelf, the probability of occurrence of these low-level inversions drops below 20% during the summer. The spatial and temporal consistency of these two parameters with the air-sea temperature difference points to the prevalence of fog on the shelf during the summer.

Analysis of surface heat fluxes show another dimension of the air-sea interaction processes involved in the fog life cycle in this area. Fog formation is associated with a positive surface latent heat flux, which is found to occur in the same spatial pattern as the fog occurrence and the negative air-sea temperature difference. The sharp negative to positive surface latent heat flux gradient across the shelfbreak shows the transition from evaporation to condensation over a relatively short spatial scale of a few degrees latitude. The surface sensible heat flux associated with fog dissipation follows this same pattern of a strong gradient along the shelf. The natural time scales of these two processes are much smaller than what can be resolved by this analysis. Since these processes are also dependent on the air-sea temperature difference, the spatial and temporal patterns follow closely.

From a climatological perspective, the consistent spatial distribution of the negative air-sea temperature differences, low-level atmospheric temperature inversions, and surface heat fluxes combined with the steady warm winds create a region with an ideal setup for advection sea fog formation. Temporally, these variables are in agreement with summer, and particularly July, being the most probable for fog in the Grand Banks, despite each variable having its own relative time-scale. The ocean is a crucial boundary condition, as the air-sea temperature difference is the main factor in fog formation in this region. The air-sea temperature difference is a product of the dynamic current interactions on the shelf from the Gulf Stream and the Labrador Current and the steady warm winds flowing from the Gulf Stream. This dynamic interaction and surface mixing leads to significant year-to-year variability in the air-sea temperature difference, which modulates fog occurrence. This variability was shown in the temporal analysis. Further studies conducted on a smaller spatial scale exploring the impact of surface shelf water mixing on fog occurrence would aid in further understanding the role of the ocean on fog dynamics.

The relationship between the ocean and fog occurrence was explored during the fog event that occurred near Sable Island. This analysis provided insight into the impact that sharp SST fronts have on fog. High-resolution satellite imagery and in-situ observations of fog structure and winds during a specific fog event show how the fog cloud was impacted by the ocean. As moist air passed over a sharp SST front, which was concurrent with the shelfbreak bathymetry, a fog cloud formed and passed over Sable Island. The fog cloud continued to build along the SST front boundary, being advected to the northwest and dissipating along the further edge from the shelfbreak. Over the 48 hour fog event, the cloud showed a strong preference for colder water, which is mostly trapped on the shelf. The behavior of the fog event is dependent on the SST front, which tends to follow the bathymetry in this region. This stresses the importance of including accurate surface boundary conditions on the submesoscale when forecasting and modeling fog.

This study ultimately finds that advection sea fog is the primary type of fog found in the

Atlantic Canada and Grand Banks region. We find that this type of fog is as dependent on ocean surface conditions as it is on favorable atmospheric conditions. Smaller-scale, accurate surface boundary conditions must be considered in modeling schemes to aid in precise forecasting of this phenomenon. We find that understanding fog dynamics in scales between the microphysical and synoptic ranges is essential.

ACKNOWLEDGEMENTS

Appendix A

A.1 ERA5 Validation

To validate the processing technique used for the binning of the ICOADS data, comparison plots were made using the ERA5 data. Figure A.1a shows the air-sea temperature difference (ΔT) from ICOADS data on a 1°grid for July 1950-2020, while Figure A.1b shows the air-sea temperature difference (ΔT) from ERA5 data on a 0.25°grid for July 1950-2020. ICOADS data is assimilated into ERA5 and combined with satellite data, hence the differences in magnitude. However, the signature of the colder water over the shelf is seen in both, following the shelfbreak bathymetry.
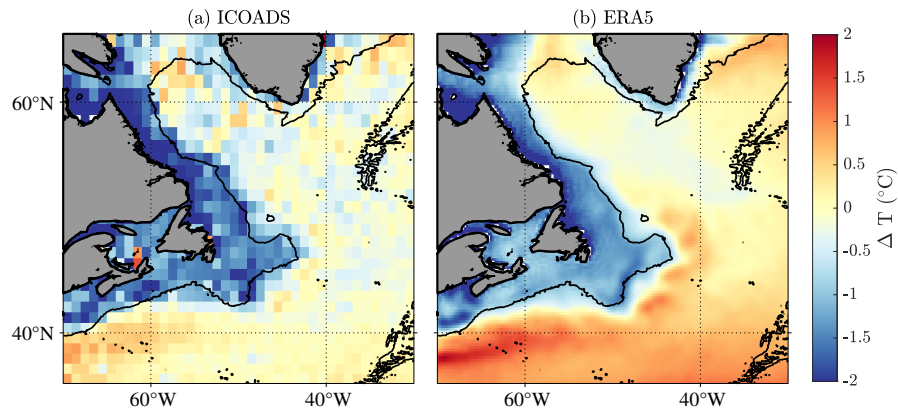

Figure A.1. Air-sea temperature difference (ΔT,°C) from (a) ICOADS data for July 1950-2020. The spatial resolution is at 1°, (b) ERA5 data for July 1950-2020. The spatial resolution is at 0.25°. The 2000 m depth contour is shown.

A.2 ICOADS Time Resolution

As noted in Table 1.1, the ICOADS observations are collected with non-uniform spacing. The observations are a combination of all records from many vessels around the region that are taking measurements at various times. The analysis done here doesn't require uniform sampling because is it being averaged over a month.

Figure A.2 shows the PDFs of the time resolution in hours as the years progress. The four ranges are 1950-1970 (red), 1970-1990 (green), 1990-2010 (purple), and 2010-2020 (blue). The most frequent sampling rate is at one hour for all time periods. In the earlier parts of the record (red and green lines), data is available at subhourly, hourly, and 3 hourly intervals. In the most recent time range (2010-2020), data is mostly available at hourly intervals.
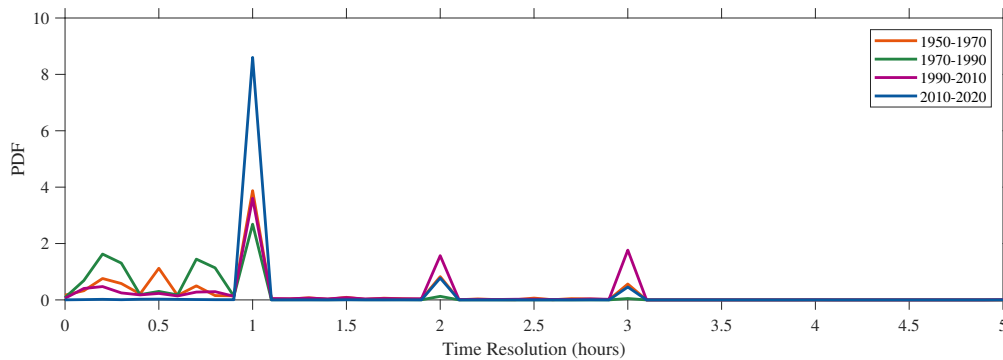

Figure A.2. A PDF of the time resolution available from ICOADS throughout the 71 year record. The spike at the hour mark signifies that most data is at hourly resolution, but also can be shorter (at every 10 or 30 minutes) or longer (every 3 hours).

A.3 ICOADS Fog and Air-Sea Temperature Difference Comparison

Figure 1.5 shows the fog occurrence and air-sea temperature difference (ΔT) side-by-side. From this perspective, areas of high fog probability are co-located with areas of negative air-sea temperature difference (ΔT). To explore this relationship further, these two variables were plotted in Figure A.3. All data is plotted in blue, while the points that were located within the "on-shelf" region (see Figure 1.11a) are plotted in mint green. From this plot, we see that fog probability increases with negative air-sea temperature difference (ΔT) values, and the points on the continental shelf are mostly within the 0 to -2°C range. Points where the fog occurrence is at 100% occurred along coasts and represent a different type of fog than the one explored in this study.
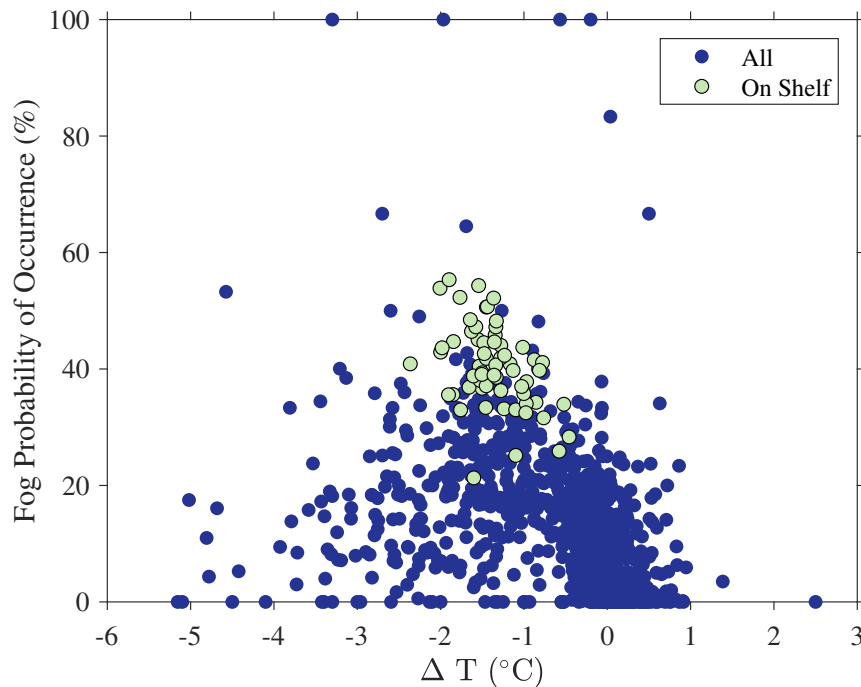

Figure A.3. Fog occurrence as a function of air-sea temperature difference (ΔT, °C) for July 1950-2020. The "on-shelf" points are in the mint green color while the rest of the data points are in blue. Note that the "on-shelf" points have higher fog percentage and negative air-sea temperature difference (ΔT) values.

Bibliography

Akimoto, Y. and Kusaka, H. (2015). A climatological study of fog in japan based on event data. *Atmospheric research*, 151:200–211.

Amani, M., Mahdavi, S., Bullock, T., and Beale, S. (2020). Automatic nighttime sea fog detection using goes-16 imagery. *Atmospheric Research*, 238:104712.

Bower, A. S., Hendry, R. M., Amrhein, D. E., and Lilly, J. M. (2013). Direct observations of formation and propagation of subpolar eddies into the subtropical north atlantic. *Deep Sea Research Part II: Topical Studies in Oceanography*, 85:15–41.

Brodrick, C. (1907). Fog on the newfoundland banks. *Monthly Weather Review*, 35(2):76–78.

Byers, H. R. (1959). *General meteorology*. McGraw-Hill.

Cardone, V. J., Greenwood, J. G., and Cane, M. A. (1990). On trends in historical marine wind data. *Journal of Climate*, 3(1):113–127.

Chen, C., Zhang, M., Perrie, W., Chang, R., Gultepe, I., Fernando, H. J., and Chen, X. (2021). A case study: Evaluation of pafog one-d model with advection in simulations of fog/stratus from c-fog experiment. *Journal of Geophysical Research: Atmospheres*, 126(20):e2021JD034812.

Chen, Z., Kwon, Y.-O., Chen, K., Fratantoni, P., Gawarkiewicz, G., and Joyce, T. M. (2020). Long-term sst variability on the northwest atlantic continental shelf and slope. *Geophysical Research Letters*, 47(1):e2019GL085455.

Clarke, R. A., Hill, H. W., Reiniger, R. F., and Warren, B. A. (1980). Current system south and east of the grand banks of newfoundland. *Journal of Physical Oceanography*, 10(1):25–65.

Dimitrova, R., Sharma, A., Fernando, H. J., Gultepe, I., Danchovski, V., Wagh, S., Bardoel, S. L., and Wang, S. (2021). Simulations of coastal fog in the canadian atlantic with the weather research and forecasting model. *Boundary-Layer Meteorology*, 181:443–472.

Dorman, C. E., Hoch, S. W., Gultepe, I., Wang, Q., Yamaguchi, R. T., Fernando, H., and Krishnamurthy, R. (2021). Large-scale synoptic systems and fog during the c-fog field experiment. *Boundary-Layer Meteorology*, 181:171–202.

Dorman, C. E., Mejia, J., Koračin, D., and McEvoy, D. (2017). Worldwide marine fog occurrence and climatology. *Marine fog: Challenges and advancements in observations, modeling, and forecasting*, pages 7–152.

Dorman, C. E., Mejia, J., Koračin, D., and McEvoy, D. (2020). World marine fog analysis based on 58-years of ship observations. *International journal of climatology*, 40(1):145–168.

Fallmann, J., Lewis, H., Sanchez, J. C., and Lock, A. (2019). Impact of high-resolution ocean–atmosphere coupling on fog formation over the north sea. *Quarterly Journal of the Royal Meteorological Society*, 145(720):1180–1201.

Fernando, H. J., Gultepe, I., Dorman, C., Pardyjak, E., Wang, Q., Hoch, S., Richter, D., Creegan, E., Gaberšek, S., Bullock, T., Hocut, C., Chang, R., Alappattu, D., Dimitrova, R., Flagg, D., Grachev, A., Krishnamurthy, R., Singh, D. K., Lozovatsky, I., Nagare, B., Sharma, A., Wagh, S., Wainwright, C., Wroblewski, M., Yamaguchi, R., Bardoel, S., Coppersmith, R. S., Chisholm, N., Gonzalez, E., Gunawardena, N., Hyde, O., Morrison, T., Olson, A., Perelet, A., Perrie, W., Wang, S., and Wauer, B. (2021). C-fog: life of coastal fog. *Bulletin of the American Meteorological Society*, 102(2):E244–E272.

Fernando, H. J., Wang, S., Huang, K. Y., and Creegan, E. (2023). Fog-laden density staircases in the marine atmospheric boundary layer. *Environmental Fluid Mechanics*, 23(2):489–510.

Findlater, J., Roach, W., and McHugh, B. (1989). The haar of north-east scotland. *Quarterly Journal of the Royal Meteorological Society*, 115(487):581–608.

Fonseca, R., Francis, D., Nelli, N., and Cherif, C. (2023). Regional atmospheric circulation patterns driving consecutive fog events in the united arab emirates. *Atmospheric Research*, 282:106506.

Fratantoni, P. S. and Pickart, R. S. (2007). The western north atlantic shelfbreak current system in summer. *Journal of Physical Oceanography*, 37(10):2509–2533.

Freeman, E., Woodruff, S. D., Worley, S. J., Lubker, S. J., Kent, E. C., Angel, W. E., Berry, D. I., Brohan, P., Eastman, R., Gates, L., Gloeden, W., Ji, Z., Lawrimore, J., Rayner, N. A., Rosenhagen, G., and Smith, S. R. (2017). Icoads release 3.0: a major update to the historical marine climate record. *International Journal of Climatology*, 37(5):2211–2232.

Grare, L., Statom, N. M., Pizzo, N., and Lenain, L. (2021). Instrumented wave gliders for air-sea interaction and upper ocean research. *Frontiers in Marine Science*, 8:664728.

Gultepe, I., Pearson, G., Milbrandt, J., Hansen, B., Platnick, S., Taylor, P., Gordon, M., Oakley, J., and Cober, S. (2009). The fog remote sensing and modeling field project. *Bulletin of the American Meteorological Society*, 90(3):341–360.

Gultepe, I., Tardif, R., Michaelides, S. C., Cermak, J., Bott, A., Bendix, J., Müller, M. D., Pagowski, M., Hansen, B., Ellrod, G., Jacobs, W., Toth, G., and Cober, S. G. (2007). Fog research: A review of past achievements and future perspectives. *Pure and applied geophysics*, 164:1121–1159.

Han, G., Ma, Z., deYoung, B., Foreman, M., and Chen, N. (2011). Simulation of three-dimensional circulation and hydrography over the grand banks of newfoundland. *Ocean Modelling*, 40(3-4):199–210.

Hersbach, H., Bell, B., Berrisford, P., Hirahara, S., Horányi, A., Muñoz-Sabater, J., Nicolas, J., Peubey, C., Radu, R., Schepers, D., Simmons, A., Soci, C., Abdalla, S., Abellan, X., Balsamo, G., Bechtold, P., Biavati, G., Bidlot, J., Bonavita, M., De Chiara, G., Dahlgren, P., Dee, D., Diamantakis, M., Dragani, R., Flemming, J., Forbes, R., Fuentes, M., Geer, A., Haimberger, L., Healy, S., Hogan, R. J., Hólm, E., Janisková, M., Keeley, S., Laloyaux, P., Lopez, P., Lupu, C., Radnoti, G., de Rosnay, P., Rozum, I., Vamborg, F., Villaume, S., and Thépaut, J.-N. (2020). The era5 global reanalysis. *Quarterly Journal of the Royal Meteorological Society*, 146(730):1999–2049.

Hu, H., Zhang, Q., Xie, B., Ying, Y., Zhang, J., and Wang, X. (2014). Predictability of an advection fog event over north china. part i: Sensitivity to initial condition differences. *Monthly Weather Review*, 142(5):1803–1822.

Hu, R. and Zhao, J. (2022). Sea surface salinity variability in the western subpolar north atlantic based on satellite observations. *Remote Sensing of Environment*, 281:113257.

Isaac, G. A., Bullock, T., Beale, J., and Beale, S. (2020). Characterizing and predicting marine fog offshore newfoundland and labrador. *Weather and Forecasting*, 35(2):347–365.

Johnstone, J. A. and Dawson, T. E. (2010). Climatic context and ecological implications of summer fog decline in the coast redwood region. *Proceedings of the National Academy of Sciences*, 107(10):4533–4538.

Koračin, D. and Dorman, C. E. (2017). *Marine fog: challenges and advancements in observations, modeling, and forecasting*. Springer.

Koračin, D., Dorman, C. E., Lewis, J. M., Hudson, J. G., Wilcox, E. M., and Torregrosa, A. (2014). Marine fog: A review. *Atmospheric Research*, 143:142–175.

Loder, J. (1998). The coastal ocean off northeastern north america: A large-scale view. *The sea*, 11:105–133.

McWilliams, J. C. (2016). Submesoscale currents in the ocean. *Proceedings of the Royal Society A: Mathematical, Physical and Engineering Sciences*, 472(2189):20160117.

Nieuwstadt, F. (2005). The atmospheric boundary layer. In *Environmental Stratified Flows*, pages 179–232. Springer.

Park, S.-Y., Yoo, J.-W., Song, S.-K., Kim, C.-H., and Lee, S.-H. (2022). Numerical study on advective fog formation and its characteristic associated with cold water upwelling. *Plos one*, 17(8):e0267895.

Pawlowicz, R. (2020). M-map: A mapping package for matlab.

Petrie, B. and Anderson, C. (1983). Circulation on the newfoundland continental shelf. *Atmosphere-Ocean*, 21(2):207–226.

Pithani, P., Ghude, S. D., Chennu, V. N., Kulkarni, R. G., Steeneveld, G.-J., Sharma, A., Prabhakaran, T., Chate, D., Gultepe, I., Jenamani, R., and Madhavan, R. (2019). Wrf model prediction of a dense fog event occurred during the winter fog experiment (wifex). *Pure and Applied Geophysics*, 176:1827–1846.

Richardson, P. L., Steele, J., Thorpe, S., and Turekian, K. (2001). Florida current, gulf stream, and labrador current. *Ocean currents*, pages 13–22.

Ricketts, N. G., Trask, P. D., Smith, E. H., Soule, F. M., Mosby, O., Institution., W. H. O., and Guard., U. S. C. (1931). *The "Marion" expedition to Davis Strait and Baffin Bay : under direction of the United States Coast Guard, 1928. Scientific results*, volume pt.1. Washington, U.S. Govt. Print. Off, 1931-37. https://www.biodiversitylibrary.org/bibliography/10182.

Scoresby, W. (1823). *Journal of a voyage to the northern whale-fishery: including researches and discoveries on the eastern coast of West Greenland, made in the summer of 1822, in the ship Baffin of Liverpool*, volume 125. Edinburgh: Printed for A. Constable.

Severini, M., Tonna, G., Moriconi, M., and Olivieri, B. (1986). Determination of the latent heat flux in fog. *Atmospheric Environment (1967)*, 20(2):397–400.

Sheng, J. and Thompson, K. R. (1996). Summer surface circulation on the newfoundland shelf and grand banks: The roles of local density gradients and remote forcing. *Atmosphere-Ocean*, 34(2):257–284.

Skyllingstad, E. D., Vickers, D., Mahrt, L., and Samelson, R. (2007). Effects of mesoscale sea-surface temperature fronts on the marine atmospheric boundary layer. *Boundary-layer meteorology*, 123:219–237.

Su, Z., Wang, J., Klein, P., Thompson, A. F., and Menemenlis, D. (2018). Ocean submesoscales

as a key component of the global heat budget. *Nature communications*, 9(1):775.

Talley, L. D. (2011). *Descriptive physical oceanography: an introduction*. Academic press.

Taylor, G. (1917). The formation of fog and mist. *Quarterly Journal of the Royal Meteorological Society*, 43(183):241–268.

Taylor, P. A., Chen, Z., Cheng, L., Afsharian, S., Weng, W., Isaac, G. A., Bullock, T. W., and Chen, Y. (2021). Surface deposition of marine fog and its treatment in the weather research and forecasting (wrf) model. *Atmospheric Chemistry and Physics*, 21(19):14687–14702.

Thomas, B. R., Kent, E. C., Swail, V. R., and Berry, D. I. (2008). Trends in ship wind speeds adjusted for observation method and height. *International Journal of Climatology: A Journal of the Royal Meteorological Society*, 28(6):747–763.

Thompson, W. T., Burk, S. D., and Lewis, J. (2005). Fog and low clouds in a coastally trapped disturbance. *Journal of Geophysical Research: Atmospheres*, 110(D18).

Tokinaga, H. and Xie, S.-P. (2011). Wave-and anemometer-based sea surface wind (waswind) for climate change analysis. *Journal of Climate*, 24(1):267–285.

Vautard, R., Yiou, P., and Van Oldenborgh, G. J. (2009). Decline of fog, mist and haze in europe over the past 30 years. *Nature Geoscience*, 2(2):115–119.

Wainwright, C. and Richter, D. (2021). Investigating the sensitivity of marine fog to physical and microphysical processes using large-eddy simulation. *Boundary-Layer Meteorology*, 181:473–498.

Willett, H. C. (1928). Fog and haze, their causes, distribution, and forecasting. *Monthly weather review*, 56(11):435–468.

WMO (2019). *Manual on Codes*. Number v. 1 in Manual on Codes. Secretariat of the World Meteorological Organization.

Yan, S., Zhu, B., and Kang, H. (2019). Long-term fog variation and its impact factors over polluted regions of east china. *Journal of Geophysical Research: Atmospheres*, 124(3):1741–1754.

Yang, Y. and Gao, S. (2020). The impact of turbulent diffusion driven by fog-top cooling on sea fog development. *Journal of Geophysical Research: Atmospheres*, 125(4):e2019JD031562.

Yang, Y., Hu, X.-M., Gao, S., and Wang, Y. (2019). Sensitivity of wrf simulations with the ysu pbl scheme to the lowest model level height for a sea fog event over the yellow sea. *Atmospheric Research*, 215:253–267.

Yun, J. and Ha, K.-J. (2022). Physical processes in sea fog formation and characteristics of turbulent air-sea fluxes at socheongcho ocean research station in the yellow sea. *Frontiers in Marine Science*, 9:825973.

Zuo, H., Balmaseda, M., Mogensen, K., Tietsche, S., and for Medium Range Weather Forecasts, E. C. (2018). *OCEAN5: The ECMWF Ocean Reanalysis System and Its Real-time Analysis Component*. ECMWF technical memoranda. European Centre for Medium-Range Weather Forecasts.